How to cite: *Angew. Chem. Int. Ed.* **2023,** *62,* e202215250
International Edition: doi.org/10.1002/anie.202215250
German Edition: doi.org/10.1002/ange.202215250

Gas Separation

Dibenzomethanopentacene-Based Polymers of Intrinsic Microporosity for Use in Gas-Separation Membranes

Jie Chen, Mariagiulia Longo, Alessio Fuoco, Elisa Esposito, Marcello Monteleone, Bibiana Comesaña Gándara, Johannes Carolus Jansen, and Neil B. McKeown**

Abstract: Dibenzomethanopentacene (DBMP) is shown to be a useful structural component for making Polymers of Intrinsic Microporosity (PIMs) with promise for making efficient membranes for gas separations. DBMP-based monomers for PIMs are readily prepared using a Diels–Alder reaction between 2,3-dimethoxyanthracene and norbornadiene as the key synthetic step. Compared to date for the archetypal PIM-1, the incorporation of DBMP simultaneously enhances both gas permeability and the ideal selectivity for one gas over another. Hence, both ideal and mixed gas permeability data for DBMP-rich co-polymers and an amidoxime modified PIM are close to the current Robeson upper bounds, which define the state-of-the-art for the trade-off between permeability and selectivity, for several important gas pairs. Furthermore, long-term studies (over ≈3 years) reveal that the reduction in gas permeabilities on ageing is less for DBMP-containing PIMs relative to that for other high performing PIMs, which is an attractive property for the fabrication of membranes for efficient gas separations.

Introduction

Polymeric gas separation membranes are of increasing use in industry for oxygen or nitrogen enrichment of air (O_2/N_2), hydrogen recovery from ammonia purge gases (H_2/N_2) and natural gas sweetening or biogas upgrading (CO_2/CH_4).[1] This is due to their low operating cost and energy consumption relative to competing technologies such as cryogenic distillation. High performing polymers for the fabrication of gas separation membranes should demonstrate high permeability (productivity) in combination with good selectivity (purity of the products).[2] However, polymeric membranes suffer from a well-known trade-off relationship between their gas permeability (P_A) and selectivity (P_A/P_B). This trade-off was first quantified by Robeson in 1991 when identifying the upper bounds for gas pairs in plots of $\log(P_A/P_B)$ versus $\log(P_A)$, which provided a benchmark of polymer performance at that time.[3] Subsequently, the positions of the gas permeability data of a new polymer relative to these upper bounds are used as a universal performance indicator to evaluate its potential performance as a separation membrane.[4]

Polymers of Intrinsic Microporosity (PIMs)[5] have emerged as promising materials for gas separation membranes.[6] In comparison to most other classes of polymer, PIMs are highly gas permeable due to the free volume created by the efficient packing of their contorted macromolecular chains and are reasonably selectivity due to their rigid fused-ring structures.[7] In 2008 gas permeability data for two PIMs derived from a spirobisindane-based monomer (PIM-1 and PIM-7) were used to redefine the Robeson upper bounds for the permeability/selectivity trade-off relationship for the majority of gas pairs.[4a] Subsequently, new PIMs with improved gas selectivity were developed by replacing the relatively flexible spirobisindane unit with more rigid structural units such as spirobifluorene,[8] ethanoanthracene,[9] triptycene,[4b,8a,10] methanopentacene[11] and Trögers base.[9a,12] In particular, data from PIMs derived from triptycene or benzotriptycene components were used to define new upper bounds for O_2/N_2, H_2/N_2 and H_2/CH_4 in 2015[4c] and, for the CO_2/N_2 and CO_2/CH_4 upper bounds in 2019.[4b] These 2019 upper bounds are of relevance to the performance of potential membranes for carbon capture and for natural gas/biogas upgrading, respectively.

As part of our continuing research programme on identifying useful rigid structural components for making PIMs, we identified the potential of the 2:1 adduct from the Diels–Alder reaction between anthracene and norbornadiene (Scheme 1). The 1:1 anthracene/norbornadiene adduct, first reported in 1975,[13] is a well-studied monomer for the preparation of high glass transition temperature polymers using ring-opening-metathesis-polymerisation (ROMP).[14] In contrast, the 2:1 adduct, given here the abbreviated name dibenzomethanopentacene (DBMP), was

[*] Dr. J. Chen, Dr. B. Comesaña Gándara, Prof. N. B. McKeown
EaStCHEM, School of Chemistry, University of Edinburgh
David Brewster Road, Edinburgh, EH9 3FJ (UK)
E-mail: neil.mckeown@ed.ac.uk
Dr. M. Longo, Dr. A. Fuoco, Dr. E. Esposito, Dr. M. Monteleone, Prof. J. Carolus Jansen
Institute on Membrane Technology, National Research Council of Italy (CNR-ITM)
via P. Bucci 17/C, 87036 Rende (CS) (Italy)
E-mail: johannescarolus.jansen@cnr.it

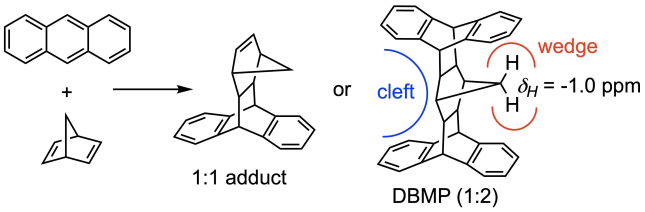

Scheme 1. The 1:1 and 2:1 (DBMP) adducts formed by the Diels–Alder reaction between anthracene and norbornadiene. Product formation is controlled by the ratio of precursors.

reported only recently.[15] It is worth noting an earlier observation of an unidentified "white solid", which was removed from the crude product of the 1:1 adduct was almost certainly DBMP.[14a] The structure of DBMP has several features that make it an attractive component for making PIMs. For example, ^{1}H NMR signals for the methylene hydrogens of DBMP are found at a highly shielded position ($\delta_H = -1.0$ ppm) due to the presence of the ring current of adjacent benzo units .[15] Therefore, this methylene bridge is likely to act as a wedge to ensure structural rigidity (Scheme 1). DBMP also possesses a large rigid cleft and other cavities, that provide intermolecular free volume similar to those of triptycene,[16] which is the structural unit for most upper bound performing PIMs. In addition, it was anticipated that DBMP-based precursors to PIM could be prepared relatively simply from the Diels–Alder reaction between an appropriate anthracene derivative and norbornadiene. In contrast, the large-scale synthesis of triptycene derivatives can be difficult due to the required generation of the highly reactive benzyne intermediate.

Results and Discussion

The target DBMP-based monomer **1** was designed for PIM synthesis using the reaction of its two catechol reactive units (i.e. 1,2-dihydroxybenzene) with 2,3,5,6-tetrafluoroterephthalonitrile (TFTPN) (Scheme 2). The required precursor to monomer **1** is 2,3-dimethoxyanthracene, which was obtained efficiently from the Friedel–Crafts acylation of phthalic anhydride with veratrole, followed by an acid-mediated cyclization and sodium borohydride reduction of the anthraquinone intermediate.[17] The Diels–Alder reaction between an excess of 2,3-dimethoxyanthracene and norbornadiene produces a crude product that is composed of three DBMP regioisomers (Scheme 2: **2a**, **2b** and **2c**)—two of which possess all four of the methoxy groups on the same side of the molecule (**2b** and **2c**) and a single isomer **2a** with the methoxy groups on opposite sides of the DBMP unit. Isomers **2b** and **2c** were deemed as undesirable as PIM precursors because a previous study indicated that similar monomers react to form small cyclic oligomers rather than high molecular mass PIMs.[18] Conveniently, the desired DBMP isomer **2a** was formed in greater yield (33 %) and was eluted first during separation by column chromatography. Isomer **2a** could be readily identified using ^{1}H NMR

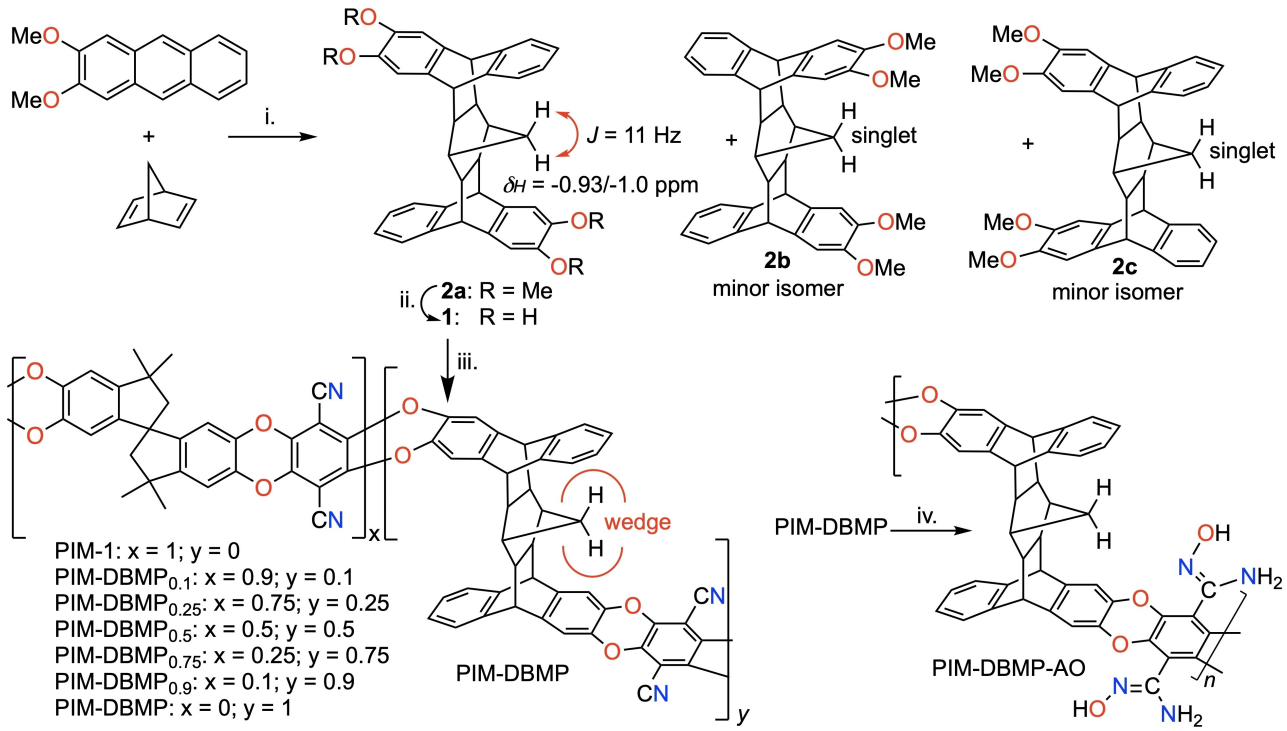

Scheme 2. The synthesis of DBMP monomer **2a** and the series of polymers prepared from it. *Reagents and conditions:* i. xylene, 260 °C, 96 h; ii. BBr_3, DCM, RT, 3 h; iii. 2,3,5,6-tetrafluoroterephthalonitrile and 5,5′,6,6′-tetrahydroxy-3,3,3′,3′-tetramethyl-spirobisindane, K_2CO_3, 65 °C, 72 h; iv. NH_2OH, NMP, 65 °C, 72 h.

spectroscopy due to the non-equivalence of the highly shielded methylene hydrogens ($\delta_H = -0.93$ and -1.00 ppm) and the large geminal coupling between them ($J_{HH} = 11$ Hz) (Figure S1). Precursor **2a** was transformed to the required biscatechol monomer **1** by a simple demethylation reaction using BBr_3 (Scheme 2). Full synthetic details are provided in the Supporting Information.

Initially a polymer, denoted as PIM-DBMP, was prepared from monomer **1** and 2,3,5,6-tetrafluoroterephthalonitrile (TFTPN) using the well-established polymerisation based on the formation of benzodioxin linkages that has often been used for PIMs synthesis.[5,19] Unfortunately, PIM-DBMP proved insoluble in most organic solvents and only partially soluble in quinoline, hence it was difficult to characterise, nevertheless, the solid state ^{13}C NMR spectrum for PIM-DBMP is consistent with its structure (Figure S2). Therefore, in order to investigate the effect of DBMP incorporation on PIM properties, co-polymers denoted as PIM-DBMP$_x$ were prepared using molar ratios of $x = 0.1$, 0.25, 0.5, 0.75 and 0.9 of DBMP monomer **1** relative to 5,5′,6,6′-tetrahydroxy-3,3,3′,3′-tetramethylspirobisindane (SBI) (i.e. the monomer used for the synthesis of PIM-1, Scheme 2).[5] In addition, modification of the nitrile groups of PIM-DBMP to amidoxime (AO) substituents,[20] to give PIM-DBMP-AO, via reaction with hydroxylamine (Scheme 2), provided solubility in the polar aprotic solvent *N*-methyl-2-pyrrolidone (NMP). It was recently reported that PIM-DBMP-AO shows promise as an ionic transport membrane for redox flow batteries.[21]

Details of the physical properties of each polymer are provided in Table 1. The copolymer PIM-DBMP$_{0.75}$ was only soluble in quinoline. In contrast, copolymers PIM-DBMP$_{0.5}$, PIM-DBMP$_{0.25}$ and PIM-DBMP$_{0.1}$ all have good solubility in $CHCl_3$ allowing analysis using gel permeation chromatography (GPC), which indicated that these polymers possess high molecular mass. Solubility in $CHCl_3$ also facilitated characterisation by ^1H NMR, which confirmed that the ratio of the incorporated DBMP component was consistent with the molar ratio of monomers used for synthesis (Figure S3).The amount of DBMP unit in each of the copolymers could also be estimated from thermal gravimetric analysis (TGA) with each DBMP-containing polymer showing commensurate weight loss at an onset temperature of 360 °C due to the release of norbornadiene through a reverse Diels–Alder reaction (Figure S4). Although the small quantity produced of each polymer (≈ 1 g) was insufficient for a full analysis of mechanical properties, atomic force microscopy (AFM) demonstrated that the Young's modulus increased with greater amounts of the more rigid DBMP component (Table 1 and Figure S5).[22]

For all DBMP containing polymers, the N_2 adsorption isotherms obtained at 77 K show high N_2 uptakes at low relative pressures ($p/p_0 < 0.1$ bar) (Figure S6), indicative of intrinsic microporosity. Apparent BET surface areas (SA_{BET}) of all copolymers in their powder form are in the range of 730–830 $m^2 g^{-1}$ similar to that of PIM-1, for which literature values are in the range 740–900 $m^2 g^{-1}$ (Table 1). The shape of each adsorption isotherm is similar to that of PIM-1, with distinct hysteresis between adsorption and desorption, which can be attributed to swelling of the polymer during N_2 uptake (Figure S6). All DBMP-containing polymers show significantly larger CO_2 uptake at 1 bar and 273 K (2.4–2.6 mmol g^{-1}) than PIM-1 (2.0 mmol g^{-1}) (Table 1, Figure S7), indicating a greater concentration of ultramicropores (< 0.7 nm). However, there is no clear trend of increasing CO_2 uptake for greater incorporation of DBMP. The modified polymer PIM-DBMP-AO demonstrates both greater SA_{BET} and CO_2 uptake at 1 bar and/273 K than the equivalent PIM-1-AO (Table 1, Figure S7).[20,23] The N_2 isotherm for PIM-DBMP-AO (Figure S6) demonstrates a relatively small degree of hysteresis between adsorption and desorption, similar to that seen for isotherms of PIM-1-AO, which is consistent with reduced swelling due to greater inter-chain cohesion from hydrogen-bonding.

Flexible and defect-free self-standing membranes of PIM-DBMP$_{0.1}$, PIM-DBMP$_{0.25}$, PIM-DBMP$_{0.5}$ were prepared by casting their $CHCl_3$ solutions, whereas PIM-DBMP$_{0.75}$ was cast from its quinoline solution (Figure S8). PIM-DBMP$_{0.9}$ and PIM-DBMP gave brittle films from quinoline, in which they are only partially soluble, however, a robust film of neat PIM-DBMP-AO could be prepared from NMP

Table 1: Physical properties of DBMP containing polymers with data for PIM-1 and PIM-1-AO included for comparison.

Polymer	M_w [g mol^{-1}]	M_w/M_n	SA_{BET}[a] [$m^2 g^{-1}$]	CO_2 uptake[b] [mmol g^{-1}]	V_{Total}[c] [mL g^{-1}]	Young's Modulus[d] [MPa]	Solubility
PIM-1	–	–	740–900	2.0	0.57	1250	$CHCl_3$
PIM-DBMP$_{0.1}$	125 000[e]	2.1	801	2.5	0.66	2400	$CHCl_3$
PIM-DBMP$_{0.25}$	71 000[e]	1.7	760	2.4	0.62	2550	$CHCl_3$
PIM-DBMP$_{0.5}$	65 000[e]	2.3	830	2.6	0.67	2870	$CHCl_3$
PIM-DBMP$_{0.75}$	–[f]	–[f]	728	2.4	0.54	3150	Quinoline
PIM-DBMP$_{0.9}$	–[f]	–[f]	817	2.4	0.73	–	Quinoline[g]
PIM-DBMP	–[f]	–[f]	790	2.4	0.73	–	Quinoline[g]
PIM-DBMP-AO	–[f]	–[f]	645	3.1	0.38	–	NMP
PIM-1-AO	–[f]	–[f]	482[20]	2.7[20]	0.27[20]	–	DMSO, NMP

[a] BET surface area (SA_{BET}) calculated from N_2 adsorption isotherm obtained at 77 K. [b] CO_2 uptakes at 1 bar and 273 K. [c] Total free volume (V_{Total}) estimated from N_2 adsorption at $p/p_0 = 0.98$. [d] Young's modulus of membranes measured by atomic force microscopy (AFM). [e] From GPC analysis relative to polystyrene standards. [f] Not measured due to insolubility in an appropriate solvent for GPC. [g] Partially soluble in quinoline.

solution. Each film, with a thickness between 88–125 μm, was treated with methanol to remove the residual casting solvent and reverse the effects of physical ageing prior to gas permeability measurements.[6]

The pure gas permeability of each film was measured initially within a day of methanol treatment, then after moderate ageing (33–140 days) and finally after long-term ageing (>2.5 years). The gas permeability coefficients and ideal gas selectivities of the novel polymers, together with those of PIM-1 and PIM-1-AO for comparison, are provided in Table 2. Data points are placed on Robeson plots for CO_2/CH_4, CO_2/N_2, O_2/N_2, H_2/N_2, H_2/CH_4 and He/N_2 (Figure 1a–f).

In direct comparison with the equivalent data for PIM-1,[8b,c] it is apparent that even the relatively small amount of DBMP within PIM-DBMP$_{0.1}$ enhances significantly both gas permeability and selectivity. The ideal selectivity tends to increase further with increasing amount of the rigid DBMP unit and is highest for PIM-DBMP$_{0.75}$. In line with the usual behaviour of PIMs, ageing of the films reduces permeability and improves selectivity. This results in data for aged films being placed well above the 2008 Robeson upper bounds. Data for PIM-DBMP$_{0.75}$ and PIM-DBMP-AO lie close to, or in some cases slightly above, the latest upper bounds (Figure 1).

The origin of the selectivity enhancement from the incorporation of the DBMP unit and the AO group was investigated by the analysis of gas diffusion coefficients (D_A, Table S1) and solubility coefficients (S_A, Table S2) obtained from the time-lag data during gas permeability measurements. Gas transport through a polymer is described by the solution-diffusion model with $P_A = D_A \times S_A$, so that selectiv-

Table 2: Membrane Thickness (l, μm), gas permeabilities (P_A, Barrer; 1 Barrer $= 10^{-10}$ $cm^3_{STP}\,cm\,cm^{-2}\,s^{-1}\,cm\,Hg^{-1}$) and ideal selectivities (P_A/P_B) of freshly methanol treated and aged films measured at 25 °C and 1 bar of feed pressure.

Polymer	l [μm]	Permeability (Barrer)						Selectivity					
		N_2	O_2	CO_2	CH_4	H_2	He	CO_2/CH_4	CO_2/N_2	O_2/N_2	H_2/N_2	H_2/CH_4	He/N_2
PIM-1[8b]	128	823	2270	13600	1360	5010	1950	10.0	16.5	2.8	6.1	3.7	2.4
(1200 days)[8c]	110	125	600	2840	159	2400	1140	17.9	22.7	4.8	19.2	15.1	9.1
PIM-DBMP$_{0.1}$	81	1000	3310	18900	1620	7810	2960	11.7	18.9	3.3	7.8	4.8	3.0
(33 days)	81	506	2120	10700	688	6460	2580	15.5	21.1	4.2	12.8	9.4	5.1
(140 days)	81	403	1780	8500	517	5860	2430	16.4	21.1	4.4	14.5	11.3	6.0
(1154 days)[a]	102	390	1580	7900	488	4560	1860	16.2	20.3	4.1	11.7	9.4	4.8
PIM-DBMP$_{0.25}$	127	1180	3880	21600	1930	8880	3270	11.2	18.3	3.3	7.5	4.6	2.8
(34 days)	127	652	2680	13200	884	7620	2940	14.9	20.2	4.1	11.7	8.6	4.5
(134 days)	127	639	2530	12200	811	6960	2690	15.0	19.0	4.0	10.9	8.6	4.2
(1156 days)[a]	121	455	1960	9680	569	5710	2230	17.0	21.3	4.3	12.6	10.3	4.9
PIM-DBMP$_{0.5}$	125	1210	4080	22200	1840	8970	3150	12.1	18.3	3.4	7.4	4.9	2.6
(118 days)	125	501	2320	11980	630	7230	2720	19.0	24.0	4.6	14.4	11.5	5.4
(1133 days)	125	503	2380	11000	637	7290	2850	17.3	22.0	4.7	14.5	11.4	5.7
(1276 days)	125	400	1970	9120	479	6680	2580	19.1	22.8	4.9	16.7	14.0	6.5
(1394 days)[b]	125	408	2126	9573	459	7784	3041	20.9	23.5	5.2	19.1	17.0	7.5
PIM-DBMP$_{0.75}$	88	827	3390	20300	1500	9530	3350	13.5	24.6	4.1	11.5	6.3	4.1
(55 days)	88	386	2130	10500	528	7920	3080	20.0	27.4	5.5	20.5	15.0	8.0
(880 days)	88	316	1640	7560	381	6660	2680	19.8	23.9	5.2	21.0	17.5	8.5
(1022 days)	88	239	1340	5970	278	5820	2400	21.5	25.0	5.6	24.4	21.0	10.0
PIM-DBMP-AO	89	106	691	3520	106	4530	1720	33.2	33.2	6.5	42.7	42.7	16.2
(70 days)	89	84	561	2910	93	3810	1420	31.4	34.6	6.7	45.1	41.1	16.8
(1011 days)	89	72	415	2260	82	2670	1080	27.6	31.2	5.7	37.0	32.6	15.0
(1152 days)	89	77	458	2290	83	2710	1070	27.6	29.7	6.0	35.1	32.6	13.8
(1267 days)[b]	89	42	262	1353	40	1839	758	33.7	32.5	6.3	44.1	45.8	18.2
PIM-1-AO[23]	90	33	147	1150	34	912	412	34.0	33.0	4.5	27.6	26.8	12.5
PIM-1-AO[24]	40	18	75.0	625	21.5	417	218	29.0	34.7	4.2	23.2	19.4	12.1

[a] Second membrane of the same polymer batch. [b] Sample tested after the mixed gas permeability measurements.

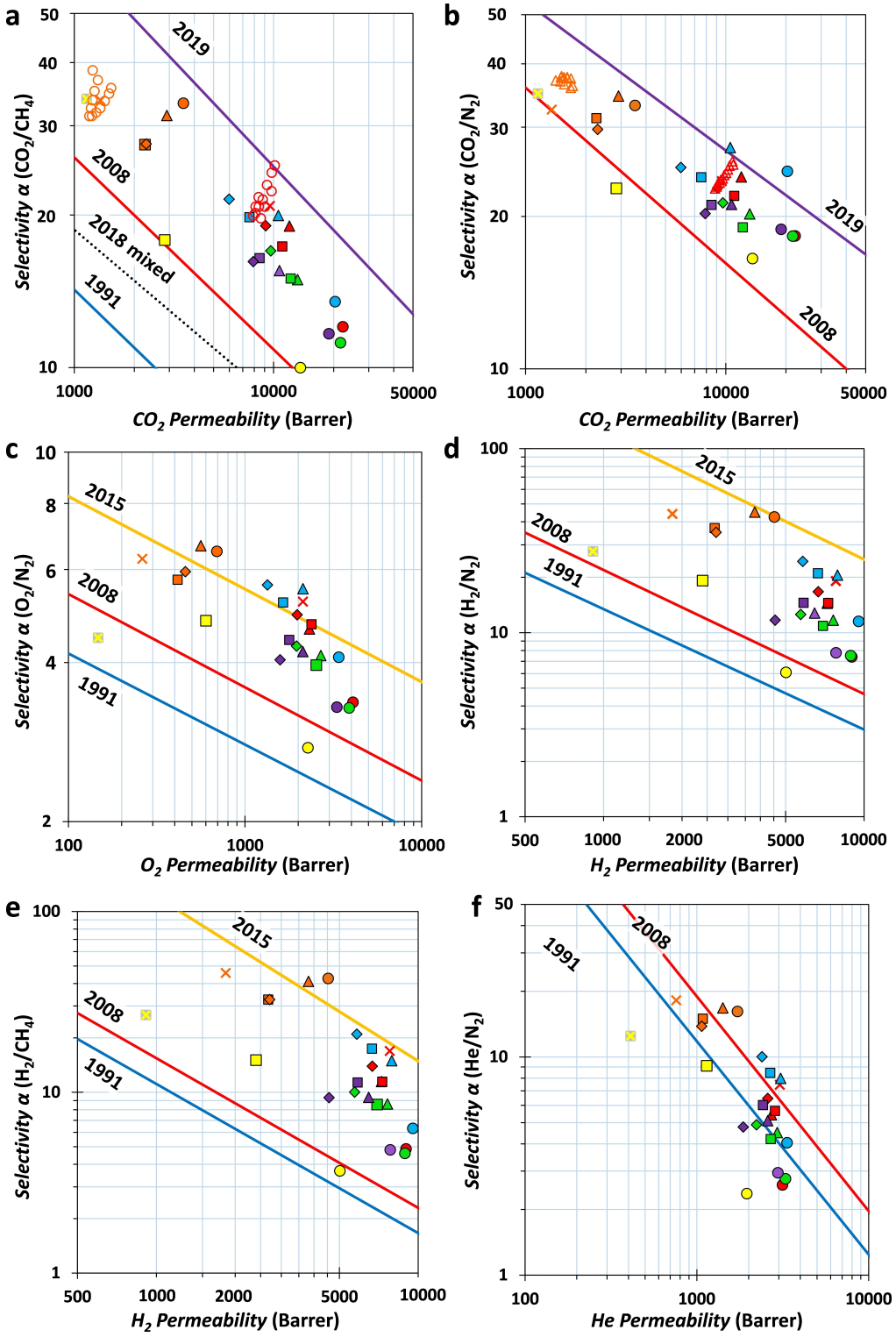

Figure 1. Robeson plots for the a) CO_2/CH_4, b) CO_2/N_2, c) O_2/N_2, d) H_2/N_2, e) H_2/CH_4 and f) He/N_2 gas pairs showing the position of the gas permeability and ideal selectivity data for films of PIM-DBMP$_{0.1}$ (●,▲,■,♦), PIM-DBMP$_{0.25}$ (●,▲,■,♦), PIM-DBMP$_{0.5}$ (●,▲,■,♦,x), PIM-DBMP$_{0.75}$ (●,▲,■,♦), PIM-DBMP-AO (●,▲,■,♦,x). All data are measured at 25 °C unless stated otherwise, and freshly MeOH treated samples are indicated as circles (○) and further aging is indicated in the order △ < □ < ◇ < x, where aged samples tested after the mixtures are indicated as (x,x). Reported data from equivalent films of PIM-1[8b,c] (●,■) and PIM-1-AO[23] (x) are shown for comparison. The groups of open symbols in the Robeson plots for CO_2/CH_4 and CO_2/N_2 represent the mixed gas permeability data from Figure 3 for PIM-DBMP$_{0.5}$ (○,△) and PIM-DBMP-AO (○,△). The upper bounds are represented by blue lines (1991), red lines (2008), yellow lines for O_2/N_2, H_2/N_2 and H_2/CH_4 (2015), purple lines for CO_2/N_2 and CO_2/CH_4 (2019), and a dashed line for CO_2/CH_4 mixtures (2018).

ity (P_A/P_B) for a polymer is the product of diffusivity selectivity (D_A/D_B) and solubility selectivity (S_A/S_B).[25] The order of decreasing diffusivity is $He > H_2 > O_2 > CO_2 > N_2 > CH_4$ as determined by the effective diameter, d_{eff},[26] of the gas molecule. It has been established that the steepness of the slope for the correlation between D_A and the square of gas effective diameter of O_2, CO_2, N_2 and CH_4 is a good indicator of the diffusivity selectivity for a polymer (Figure 2).[26] For PIMs this slope is characteristically different for the small molecules He and H_2, as reported previously.[27] Clearly, the He and H_2 diffusivity is significantly higher in all copolymers than in PIM-1, most likely due to a more interconnected free volume network in the copolymers. The slope of D vs. d^2_{eff} is steeper for the PIM copolymer PIM-DBMP$_{0.75}$ containing the highest ratio of DBMP to SBI units and is even greater for PIM-DBMP-AO. This enhanced molecular sieving is attributable to the greater rigidity of the DBMP unit relative to that of the SBI unit. These values for diffusion selectivity are similar to those observed for the upper bound-defining triptycene-based PIMs and arise from the restricted transport of a larger gas molecule through the rigid polymer matrix.[4b] Transport of larger gas molecules involves a hopping mechanism from one element of free volume to another and requires greater thermal energy for the necessary opening to occur via vibrations of the rigid polymer.[4b,25,27] Increasing diffusion selectivity on aging is the main cause of the enhanced ideal gas selectivity and this can be attributed to preferential loss of larger free volume elements (>0.7 nm) over those of smaller diameter.

Generally, the gas solubilities are high, a common feature for all PIMs, and the particularly high values of CO_2 solubility, followed by those of CH_4 (Table S2), are reflected

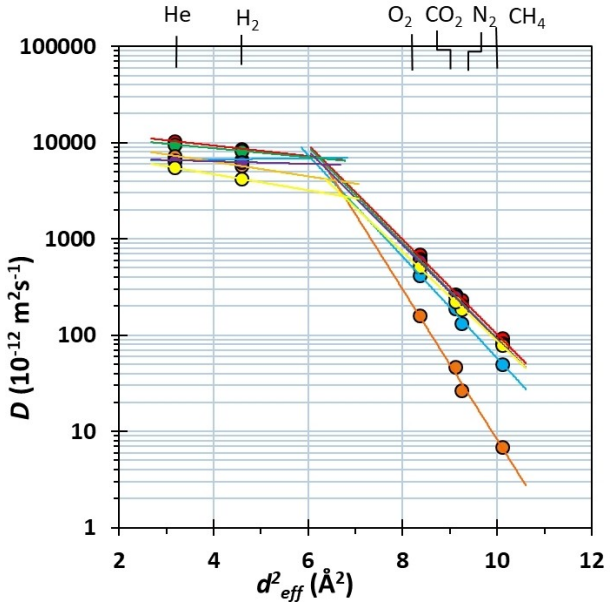

Figure 2. Correlation of diffusivity coefficient (D_A) with the squared effective gas diameter (d^2_{eff}) of gas molecule (He = 1.78, H_2 = 2.14, O_2 = 2.89, CO_2 = 3.02, N_2 = 3.04, CH_4 = 3.18 Å)[26] for freshly methanol treated films of PIM-DBMP$_{0.1}$ (●), PIM-DBMP$_{0.25}$ (●), PIM-DBMP$_{0.5}$ (●), PIM-DBMP$_{0.75}$ (●), PIM-DBMP-AO (●), and PIM-1 (●).

in the order of decreasing gas permeabilities being $CO_2 > H_2 > O_2 > He > CH_4 > N_2$ for all the PIM-DBMP copolymers. In most cases, the solubility selectivity remains constant as the ratio of DBMP to SBI units increases and as the films age. The exceptionally high values for S_{CO_2} are related to the amount of free volume present in the polymer (i.e. intrinsic microporosity). Therefore, its loss during prolonged aging causes a decrease in S_{CO_2}. For the CO_2/N_2 gas pair, the high permselectivity is predominantly due to the large difference in solubility, and P_{CO_2}/P_{N_2} is thus proportional to S_{CO_2}/S_{N_2} with D_{CO_2}/D_{N_2} being close to unity (Table S1). Therefore, ageing of the films provides a lower contribution of solubility to the overall ideal selectivity (P_{CO_2}/P_{N_2}). This is especially the case for PIMs with high DBMP content, where long-term ageing significantly reduces P_{CO_2}/P_{N_2}. Similar ageing behaviour has been observed for other PIMs based on rigid structural units.[8c]

For PIM-DBMP-AO, the initial gas permeability is much lower but the ideal selectivity is higher with respect to the other DBMP-based PIMs. This can be explained by the polymer possessing a much denser initial state after methanol treatment, induced by the greater inter-chain cohesion due to extensive hydrogen bonding between the amidoxime groups.[23] This leads to slower gas diffusion but more pronounced size-sieving properties, highlighted by the much steeper slope in Figure 2.

Physical ageing is a general feature of glassy polymers, in which the polymer develops a more tightly packed state leading to a reduction in gas permeability. For high free volume polymers such as PIMs the permeability reduction can be very large. Extended studies (>1000 days) were conducted on the films to investigate the impact of the DBMP unit on gas permeability (Table 2). Overall, the gas permeability reduction for the DBMP copolymer films is in the range 36–50 %, which is significantly less than that of a similar film of PIM-1 (74 %) and a similarly deep-aged film of a spirobifluorene-based PIM (PIM-SBF-1; 66 %).[8c] This suggests that the incorporation of DBMP units significantly slows physical ageing of the films. Long-term ageing of the PIM-DBMP-AO film results in only a small overall reduction in gas permeabilities but, unusually, the loss of permeability is greater for smaller gas molecules (He and H_2) due to a significant reduction of their diffusivity (Figure S9). This results in a relatively small decrease in selectivity, which is likely to be associated with loss of small elements of free volume (<0.7 nm). This unusual ageing behaviour appears to be related to the AO modification and this should be investigated for other AO-modified PIMs. Nevertheless, data for the long-term aged film of PIM-DBMP-AO are still impressive (e.g. P_{O_2} = 262 Barrer; P_{O_2}/P_{N_2} = 6.3) especially in comparison with those of PIM-1-AO.

Based on the pure gas permeabilities and ideal selectivities, we envisage the potential application of these membranes in biogas upgrading or in CO_2 capture from flue gas. The mixed gas permeability was therefore measured up to 6 bar with mixtures of CO_2/CH_4 (35/65 vol %) and CO_2/N_2 (15/85 vol %), representative for biogas and CO_2 rich flue gas, respectively, using our previously reported customized setup.[28] Under much harsher conditions, with high pres-

sures and CO_2 rich gas streams, PIMs are known to be subject not only to physical aging, as already discussed above for the single gases, but also to plasticization.[29] Weaker effects were also observed in this work, where PIM-DBMP-AO shows a slight hysteresis between the pressure-increase steps and the subsequent pressure-decrease steps for CO_2/CH_4 (Figure 3a) and CO_2/N_2 mixtures (Figure 3c), in both cases with an increase in permeability during depressurization, and only for CO_2/CH_4 a slight loss in selectivity. This suggests a weak dilation of the membrane upon exposure to the higher CO_2 partial pressures (concentrations), which is not recovered on the time scale of the measurements, due to the slow chain dynamics of the very rigid ladder polymers. Instead, PIM-DBMP$_{0.5}$ only shows hysteresis for the CO_2/CH_4 mixture (Figure 3b), but in this case the CO_2 permeability slightly increases and the CH_4 permeability decreases, resulting in a somewhat higher selectivity after exposure to the higher CO_2 partial pressures. This suggests a simultaneous dilation (favouring CO_2 permeation) and physical aging (affecting negatively especially the larger CH_4 molecules), probably resulting in a narrowing of the bottle necks between the free volume elements.[27]

In all cases, the CO_2 permeability tends to decrease with increasing pressure for the CO_2/CH_4 (35/65 vol %) mixture and the CO_2/N_2 (15/85 vol %) mixture, as already observed under similar conditions for other PIMs, such as PIM-2,[30] but this decrease is much stronger in PIM-DBMP$_{0.5}$ than in PIM-DBMP-AO. Especially for the CO_2/CH_4 mixture, it also leads to a modest decrease in the selectivity, whereas for the CO_2/N_2 (15/85 vol %) mixture the decrease in selectivity is only observed in PIM-DBMP$_{0.5}$. The decrease

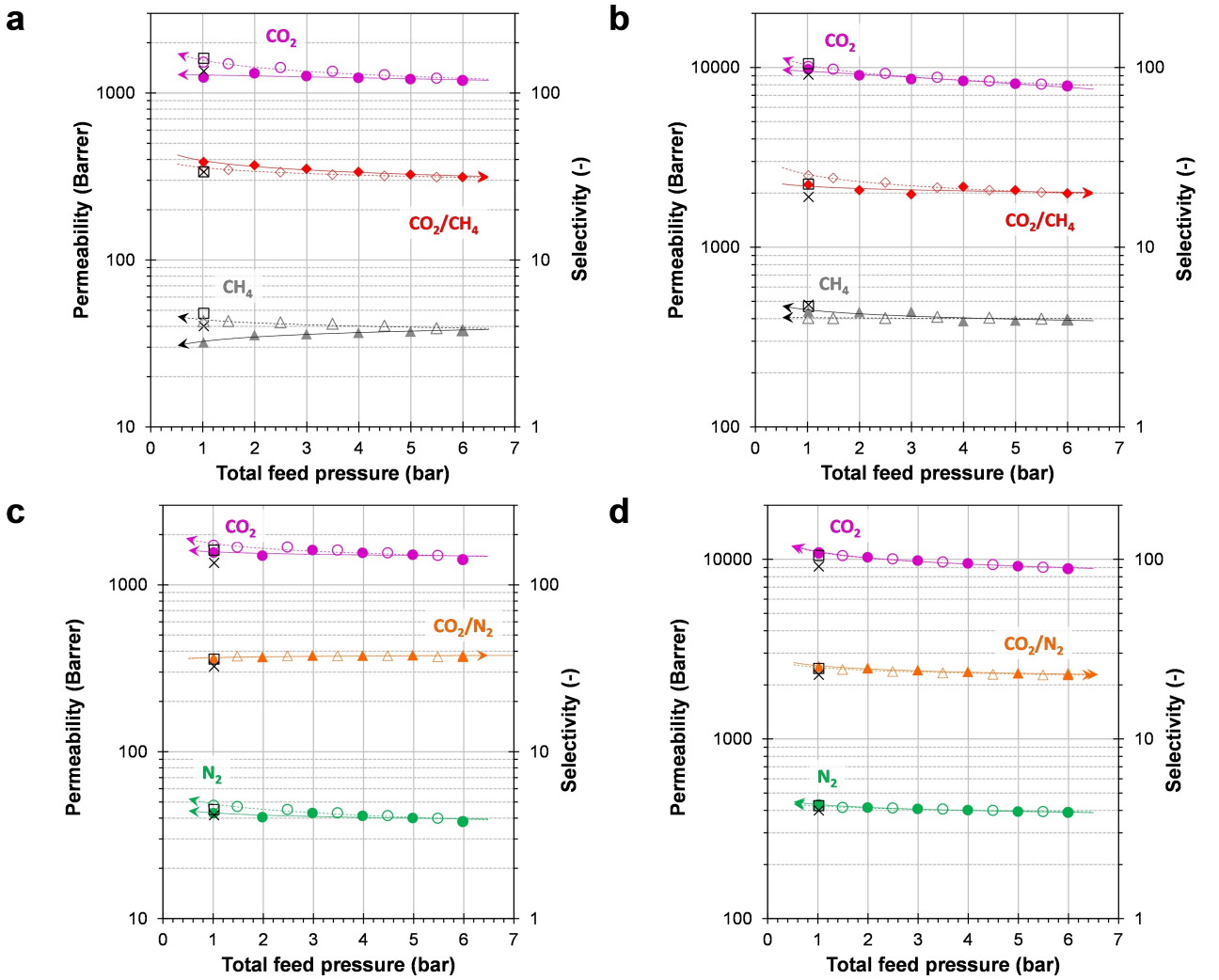

Figure 3. Mixed gas permeability of CO_2(●,■) CH_4, (♦, ◇) N_2 (●, ■) and selectivity of CO_2/CH_4 (35/65 Vol%; ♦, ◇) and CO_2/N_2 (15/85 Vol%; ▲, △) mixtures in PIM-DBMP-AO (a, c) and PIM-DBMP$_{0.5}$ (b, d). Solid symbols represent the increasing pressure steps and open symbols the subsequent decreasing pressure steps. Single gas permeabilities at 1 bar in the mixed gas setup (□), are shown for comparison and show the nearly perfect overlap with the mixed gas permeation data on the same setup. Single gas permeabilities at 1 bar in the fixed volume time lag setup are also reported for comparison between the two methods (x). Lines are plotted as a guide to the eye and the arrows point towards the axis where to read the data. The maximum stage cut is $CO_2 < 1.5$ %, $N_2 < 0.65$ % and $CH_4 < 0.65$ % in PIM-DBMP$_{0.5}$, and $CO_2 < 0.45$ %, $N_2 < 0.01$ % and $CH_4 < 0.008$ % in PIM-DBMP-AO.

in permeability is a typical consequence of the dual mode sorption mechanism, while at higher pressures than those used in this work, plasticization may lead to more complex phenomena, such as an increase of CO_2 permeability with pressure and a subsequent decrease with time[31] and usually a reduction of the mixed gas selectivity at higher pressures,[1c] although an increase in selectivity has also been observed for PIMs with particularly favourable competitive sorption.[32] The mixed gas permeability data for PIM-DBMP$_{0.5}$ are similar to that obtained from single gas measurements and close to the proposed 2019 CO_2/CH_4 and CO_2/N_2 upper bounds (Figure 1a and b). PIM-DBMP-AO also exhibits a promising performance in mixed gas measurements, locating far above the 2018 CO_2/CH_4 upper bound for mixed gas[1c] (Figure 1a). For comparison, the single gas permeation measurements, determined on the same cross-flow apparatus (Figure 3, □), show minor differences with the mixed gas permeation measurements. Instead, the measurements on the fixed volume time lag apparatus (Figure 3, ×) are systematically lower in both polymers, especially for CO_2 (10–20 %), resulting in a slightly lower ideal selectivity as well. This is most likely due to the different measurement principle in the two instruments, but may in part also be a result of the sample history, since measurements in the fixed volume setup were done after the entire cycle with the gas mixtures.

Conclusion

The recently reported DBMP unit is shown to be a useful structural component for making PIMs that show promise for the fabrication of gas separation membranes. Synthesis of the key DBMP monomer **1** is relatively straightforward and could be more easily carried out on a large scale relative to that of triptycene based monomers that provide high performance PIMs. Despite the lack of solubility for the homopolymer PIM-DBMP in organic solvents, the amidoxime modified derivative (PIM-DBMP-AO) proved soluble in NMP from which robust films could be cast. Incorporation of the DBMP unit into random copolymers with SBI units also provided samples that could be cast as films from chloroform solution. These films show that DBMP incorporation enhances both permeability and selectivity relative to PIM-1 and suggests that DBMP has a similar beneficial effect on performance as triptycene or benzotriptycene as a structural unit. From a practical perspective, the co-polymer PIM-DBMP$_{0.5}$ provides an excellent compromise between performance (i.e. near to the upper bound for several gas pairs) and ease of processability (i.e. freely soluble in chloroform). PIM-DBMP$_{0.50}$ would also be more cost-effective due to the use of the inexpensive SBI co-monomer in its synthesis. The membranes maintain most of their excellent performance under mixed gas permeation conditions with CO_2/CH_4 and CO_2/N_2 mixtures, opening interesting perspectives in biogas upgrading and carbon capture from CO_2 rich flue gas.

Acknowledgements

Prof. M. P. De Santo (University of Calabria) is gratefully acknowledged for help with the AFM force spectroscopy measurements. The project is partially sponsored by the Department of the Defence Threat Reduction Agency grant number HDTRA1-18-1-0054.

Conflict of Interest

The authors declare no conflict of interest.

Data Availability Statement

The data that support the findings of this study are available in the Supporting Information of this article.

Keywords: Ageing · Dibenzomethanopentacene · Gas Separation · Membranes · Polymers of Intrinsic Microporosity

[1] a) S. Wang, X. Li, H. Wu, Z. Tian, Q. Xin, G. He, D. Peng, S. Chen, Y. Yin, Z. Jiang, M. D. Guiver, *Energy Environ. Sci.* **2016**, *9*, 1863–1890; b) D. S. Sholl, R. P. Lively, *Nature* **2016**, *532*, 435–437; c) Y. Wang, X. Ma, B. S. Ghanem, F. Alghunaimi, I. Pinnau, Y. Han, *Mater. Today Nano* **2018**, *3*, 69–95; d) Y. Yampolskii, *Macromolecules* **2012**, *45*, 3298–3311; e) E. Esposito, L. Dellamuzia, U. Moretti, A. Fuoco, L. Giorno, J. C. Jansen, *Energy Environ. Sci.* **2019**, *12*, 281–289.

[2] a) P. M. Budd, N. B. McKeown, *Polym. Chem.* **2010**, *1*, 63–68; b) S. Kim, Y. M. Lee, *Prog. Polym. Sci.* **2015**, *43*, 1–32; c) A. F. Bushell, P. M. Budd, M. P. Attfield, J. T. A. Jones, T. Hasell, A. I. Cooper, P. Bernardo, F. Bazzarelli, G. Clarizia, J. C. Jansen, *Angew. Chem. Int. Ed.* **2013**, *52*, 1253–1256; *Angew. Chem.* **2013**, *125*, 1291–1294.

[3] a) L. M. Robeson, *J. Membr. Sci.* **1991**, *62*, 165–185; b) B. D. Freeman, *Macromolecules* **1999**, *32*, 375–380.

[4] a) L. M. Robeson, *J. Membr. Sci.* **2008**, *320*, 390–400; b) B. Comesaña-Gándara, J. Chen, C. G. Bezzu, M. Carta, I. Rose, M.-C. Ferrari, E. Esposito, A. Fuoco, J. C. Jansen, N. B. McKeown, *Energy Environ. Sci.* **2019**, *12*, 2733–2740; c) R. Swaidan, B. Ghanem, I. Pinnau, *ACS Macro Lett.* **2015**, *4*, 947–951.

[5] P. M. Budd, B. S. Ghanem, S. Makhseed, N. B. McKeown, K. J. Msayib, C. E. Tattershall, *Chem. Commun.* **2004**, 230–231.

[6] N. B. McKeown, *Polymer* **2020**, *202*, 122736.

[7] a) N. B. McKeown, *Curr. Opin. Chem. Eng.* **2022**, *36*, 100785; b) Y. Wang, B. S. Ghanem, Y. Han, I. Pinnau, *Curr. Opin. Chem. Eng.* **2022**, *35*, 100755; c) X. Chen, L. Wu, H. Yang, Y. Qin, X. Ma, N. Li, *Angew. Chem. Int. Ed.* **2021**, *60*, 17875–17880; *Angew. Chem.* **2021**, *133*, 18019–18024.

[8] a) C. G. Bezzu, A. Fuoco, E. Esposito, M. Monteleone, M. Longo, J. C. Jansen, G. S. Nichol, N. B. McKeown, *Adv. Funct. Mater.* **2021**, *31*, 2104474; b) C. G. Bezzu, M. Carta, A. Tonkins, J. C. Jansen, P. Bernardo, F. Bazzarelli, N. B. McKeown, *Adv. Mater.* **2012**, *24*, 5930–5933; c) C. G. Bezzu, M. Carta, M. C. Ferrari, J. C. Jansen, M. Monteleone, E. Esposito, A. Fuoco, K. Hart, T. P. Liyana-Arachchi, C. M. Colina, N. B. McKeown, *J. Mater. Chem. A* **2018**, *6*, 10507–10514.

[9] a) M. Carta, R. Malpass-Evans, M. Croad, Y. Rogan, J. C. Jansen, P. Bernardo, F. Bazzarelli, N. B. McKeown, *Science* **2013**, *339*, 303–307; b) Y. Rogan, R. Malpass-Evans, M. Carta,

M. Lee, J. C. Jansen, P. Bernardo, G. Clarizia, E. Tocci, K. Friess, M. Lanc, N. B. McKeown, *J. Mater. Chem. A* **2014**, *2*, 4874–4877; c) X. Ma, I. Pinnau, *Macromolecules* **2018**, *51*, 1069–1076.

[10] a) B. S. Ghanem, R. Swaidan, E. Litwiller, I. Pinnau, *Adv. Mater.* **2014**, *26*, 3688–3692; b) R. Swaidan, M. Al-Saeedi, B. Ghanem, E. Litwiller, I. Pinnau, *Macromolecules* **2014**, *47*, 5104–5114; c) I. Rose, M. Carta, R. Malpass-Evans, M. C. Ferrari, P. Bernardo, G. Clarizia, J. C. Jansen, N. B. McKeown, *ACS Macro Lett.* **2015**, *4*, 912–915; d) B. S. Ghanem, F. Alghunaimi, Y. G. Wang, G. Genduso, I. Pinnau, *ACS Omega* **2018**, *3*, 11874–11882; e) G. Genduso, B. S. Ghanem, Y. Wang, I. Pinnau, *Polymer* **2019**, *11*, 361; f) T. Zhang, L. Deng, P. Li, *Ind. Eng. Chem. Res.* **2020**, *59*, 18640–18648; g) X. Ma, Z. Zhu, W. Shi, W. Ji, J. Li, Y. Wang, I. Pinnau, *J. Mater. Chem. A* **2021**, *9*, 5404–5414.

[11] R. Williams, L. Burt, E. Esposito, J. Jansen, E. Tocci, C. Rizzuto, M. Lanč, M. Carta, N. McKeown, *J. Mater. Chem. A* **2018**, *6*, 5661–5667.

[12] a) Z. Zhu, J. Zhu, J. Li, X. Ma, *Macromolecules* **2020**, *53*, 1573–1584; b) X. Ma, H. W. H. Lai, Y. Wang, A. Alhazmi, Y. Xia, I. Pinnau, *ACS Macro Lett.* **2020**, *9*, 680–685; c) R. Malpass-Evans, I. Rose, A. Fuoco, P. Bernardo, G. Clarizia, N. B. McKeown, J. C. Jansen, M. Carta, *Membranes* **2020**, *10*, 62.

[13] D. N. Butler, A. Barrette, R. A. Snow, *Synth. Commun.* **1975**, *5*, 101–106.

[14] a) M. Hong, L. Cui, S. R. Liu, Y. S. Li, *Macromolecules* **2012**, *45*, 5397–5402; b) J. X. Yang, J. Cui, Y. Y. Long, Y. G. Li, Y. S. Li, *J. Polym. Sci. Part A* **2014**, *52*, 2654–2661.

[15] S. V. Shorunov, M. A. Rudakova, M. E. Fil'kina, Y. V. Nelyubina, M. V. Bermeshev, *Pet. Chem.* **2019**, *59*, S88–S94.

[16] a) T. M. Long, T. M. Swager, *Adv. Mater.* **2001**, *13*, 601–604; b) N. T. Tsui, A. J. Paraskos, L. Torun, T. M. Swager, E. L. Thomas, *Macromolecules* **2006**, *39*, 3350–3358.

[17] a) J. L. Pozzo, G. M. Clavier, M. Colomes, H. Bouas-Laurent, *Tetrahedron* **1997**, *53*, 6377–6390; b) T. J. Corrado, Z. Huang, D. Huang, N. Wamble, T. Luo, R. Guo, *Proc. Natl. Acad. Sci. USA* **2021**, *118*, e2022204118.

[18] R. Short, M. Carta, C. G. Bezzu, D. Fritsch, B. M. Kariuki, N. B. McKeown, *Chem. Commun.* **2011**, *47*, 6822–6824.

[19] N. B. McKeown, *Sci. China Chem.* **2017**, *60*, 1023–1032.

[20] H. A. Patel, C. T. Yavuz, *Chem. Commun.* **2012**, *48*, 9989–9991.

[21] C. Ye, R. Tan, A. Wang, J. Chen, B. Comesaña Gándara, C. Breakwell, A. Alvarez-Fernandez, Z. Fan, J. Weng, C. G. Bezzu, S. Guldin, N. P. Brandon, A. R. Kucernak, K. E. Jelfs, N. B. McKeown, Q. Song, *Angew. Chem. Int. Ed.* **2022**, *61*, e202207580; *Angew. Chem.* **2022**, *134*, e202207580.

[22] a) K. Polak-Kraśna, C. Fuhrhop, S. Rochat, A. D. Burrows, A. Georgiadis, C. R. Bowen, T. J. Mays, *Int. J. Hydrogen Energy* **2017**, *42*, 23915–23919; b) M. Longo, M. P. De Santo, E. Esposito, A. Fuoco, M. Monteleone, L. Giorno, B. Comesana-Gandara, J. Chen, C. G. Bezzu, M. Carta, I. Rose, N. B. McKeown, J. C. Jansen, *Ind. Eng. Chem. Res.* **2020**, *59*, 5381–5391.

[23] R. Swaidan, B. S. Ghanem, E. Litwiller, I. Pinnau, *J. Membr. Sci.* **2014**, *457*, 95–102.

[24] M. Longo, B. Comesaña-Gándara, M. Monteleone, E. Esposito, A. Fuoco, L. Giorno, N. B. McKeown, J. C. Jansen, *J. Membr. Sci. Res.* **2022**, *8*, 540493.

[25] A. Fuoco, B. Comesana-Gandara, M. Longo, E. Esposito, M. Monteleone, I. Rose, C. G. Bezzu, M. Carta, N. B. McKeown, J. C. Jansen, *ACS Appl. Mater. Interfaces* **2018**, *10*, 36475–36482.

[26] V. Teplyakov, P. Meares, *Gas Sep. Purif.* **1990**, *4*, 66–74.

[27] A. Fuoco, C. Rizzuto, E. Tocci, M. Monteleone, E. Esposito, P. M. Budd, M. Carta, B. Comesaña-Gándara, N. B. McKeown, J. C. Jansen, *J. Mater. Chem. A* **2019**, *7*, 20121–20126.

[28] S. C. Fraga, M. Monteleone, M. Lanč, E. Esposito, A. Fuoco, L. Giorno, K. Pilnáček, K. Friess, M. Carta, N. B. McKeown, P. Izák, Z. Petrusová, J. G. Crespo, C. Brazinha, J. C. Jansen, *J. Membr. Sci.* **2018**, *561*, 39–58.

[29] R. Swaidan, B. Ghanem, E. Litwiller, I. Pinnau, *Macromolecules* **2015**, *48*, 6553–6561.

[30] A. Fuoco, B. Satilmis, T. Uyar, M. Monteleone, E. Esposito, C. Muzzi, E. Tocci, M. Longo, M. P. D. Santo, M. Lanč, K. Friess, O. Vopička, P. Izák, J. C. Jansen, *J. Membr. Sci.* **2020**, *594*, 117460.

[31] R. R. Tiwari, J. Jin, B. D. Freeman, D. R. Paul, *J. Membr. Sci.* **2017**, *537*, 362–371.

[32] K. Mizrahi Rodriguez, F. M. Benedetti, N. Roy, A. X. Wu, Z. P. Smith, *J. Mater. Chem. A* **2021**, *9*, 23631–23642.

Manuscript received: October 17, 2022
Accepted manuscript online: December 13, 2022
Version of record online: January 16, 2023